Development of advanced in-situ EP diagnostic tools at IOM: Current status

IEPC-2017-441

Presented at the 35th International Electric Propulsion Conference
Georgia Institute of Technology • Atlanta, Georgia • USA
October 8 – 12, 2017

C. Bundemann[1], F. Scholze[2], C. Eichhorn[3], D. Spemann[4], and H. Neumann[5]
Leibniz-Institute of Surface Modification, Permoserstr. 15, 04318 Leipzig, Germany

F. Scortecci[6]
Aerospazio Tecnologie s.r.l., Via Provinciale Nord 42a, 53040 Rapolano Terme, Siena, Italy

H. J. Leiter[7]
ArianeGroup GmbH, Im Langen Grund, 74239 Hardthausen-Lampoldshausen, Germany

and

K. Holste[8] and P. J. Klar[9]
Justus-Liebig-Universität Gießen, Heinrich-Buff-Ring 16, 35392 Gießen, Germany

Abstract: Reliable and reproducible characterization of EP thrusters is a key factor in the development and qualification process. This paper reports on intensive activities related to the development of advanced in-situ characterization tools that are likely to serve as a reference. The research activities at the Leibniz-Institute of Surface Modification (IOM) focus on the development and improvement of measurement sensors for ion beam and plasma characterization, optical inspection and thermal characterization. The tools comprise Faraday probe and retarding potential analyzer, high-resolution optical telemicroscope and triangular laser head, pyrometer and thermocamera. All probes are operated in-vacuum. Some of them are commercial devices that are not specified for operation in vacuum. In the latter case, the design has been modified in order to grant successful in-vacuum operation. The sensors are part of the Advanced Electric Propulsion Diagnostics (AEPD) system. Test measurements were performed with two EP thrusters, a gridded ion thruster RIT-µX and a Hall effect thruster SPT-100. The results demonstrate impressively the capabilities of the AEPD system, i.e. the possibility to get in-situ a comprehensive set of thruster performance parameters.

[1] Senior scientist, carsten.bundesmann@iom-leipzig.de.
[2] Senior scientist, frank.scholze@iom-leipzig.de.
[3] Senior scientist, christoph.eichhorn@iom-leipzig.de.
[4] Senior scientist and group leader, daniel.spemann@iom-leipzig.de.
[5] Senior scientist, horst.neumann@iom-leipzig.de.
[6] CEO and senior scientist, fscortecci@aerospazio.com.
[7] Professor and group leader, hans.leiter@ariane.group.
[8] Senior scientist, Kristof.Holste@exp1.physik.uni-giessen.de.
[9] Professor and group leader, Peter.J.Klar@exp1.physik.uni-giessen.de.

Nomenclature

d	=	distance
h	=	height
I	=	current
t	=	transmission
T	=	temperature
U	=	voltage
x	=	coordinate of the positioning system
λ	=	wavelength of light

I. Introduction

Recently, we have set up an Advanced Electric Propulsion Diagnostic (AEPD) platform [1], which facilitates for the in-situ measurement of a comprehensive set of thruster performance parameters. The platform utilizes a five-axis-movement system for precise positioning of the thruster with respect to the diagnostic heads. In the first setup (AEPD1) an energy-selective mass spectrometer (ESMS) and a miniaturized Faraday probe for ion beam characterization, a telemicroscope and a triangular laser head for measuring the erosion of mechanical parts, and a pyrometer for surface temperature measurements were integrated. The capabilities of the AEPD1 platform were demonstrated with two electric propulsion thrusters, a gridded ion thruster RIT-22 (ArianeGroup, [1-3]) and a Hall effect thruster SPT-100D EM1 (EDB Fakel, Russia, [1,4]), in two different space simulation (vacuum) facilities.

Despite the successful verification of the potential of the AEPD1 platform, the tests revealed some severe problems. Firstly, the dimension of some of the diagnostic heads is in the order of the size of the exit plane of the tested thrusters. Thus, the interaction of diagnostic heads and energetic particle beam is rather large. Secondly, some of the diagnostic heads were placed inside vacuum sealed housings equipped with appropriate windows for safety reasons. Because of that, there is a certain risk that the window might break, when the housing is brought into the energetic particle beam. Breaking the window would result in a vacuum breakdown with the severe danger that the thruster or other devices might get damaged.

In order to overcome these problems, we are currently testing a new setup (AEPD2) [5,6], which utilizes modified (telemicroscope, triangular laser head), alternative (pyrometer) or additional diagnostic heads (thermocamera, retarding potential analyzer) [7,8]. The goal is to operate all diagnostic heads in-vacuum. Doing so, we can reduce the dimension of the diagnostic heads considerably and eliminate the risk of a vacuum breakdown. Furthermore, the new diagnostic heads extend the variety of implemented measurement techniques (thermal imaging with thermocamera) or provide a low-cost alternative to existing devices (retarding potential analyzer instead of the ESMS). Here, we describe the design of the diagnostic heads developed at the Leibniz-Institute of Surface Modification (IOM) and present first experimental results, exemplary, with a gridded ion thruster RIT-µX.

II. Experimental

A. Telemicroscope

The telemicroscope is used for high-resolution optical imaging. Taking images allows, for instance, measuring the erosion of mechanical parts [2,4]. The telemicroscope consists of a CCD camera, an extension tube, a photographic lens, and high-power LEDs for illumination. The first setup of the telemicroscope used a vacuum-sealed housing with a shutter and high-power LEDs. The setup worked fine [1,2,4] but the dimension was rather large: 120 mm in diameter and 500 mm in length. The new design (see Figure 1) uses only a cover made of metal, which eliminates the risk of a vacuum failure. The camera is now operated inside vacuum, even though it is not specified for in-vacuum operation. The new design reduces the dimension considerably. Thus, the interaction with the thruster is reduced.

The performance of the optical system depends on the focal length of the photographic lens, the length of the extension tube, and the parameters of the CCD chip (resolution and pixel size). Using simple equations from physical optics allows calculating the performance parameters. Figure 2 shows, exemplary, calculated and measured results for a setup with a lens with a focal length of f = 50 mm and different extension tube lengths. There is a very good agreement between calculated and measured data. The goal was to develop a setup, which is as small as possible and has a lateral resolution of better than 10 µm. Therefore, we chose a lens with f = 50 mm and an extension tube length of 40 mm.

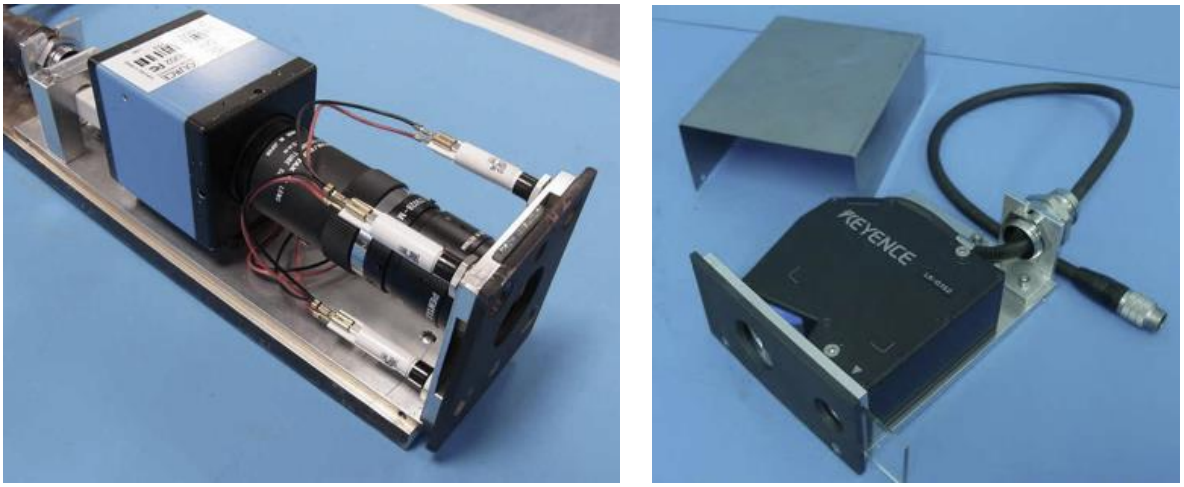

Figure 1: Telemicroscope (left) and triangular laser head (right) with housing.

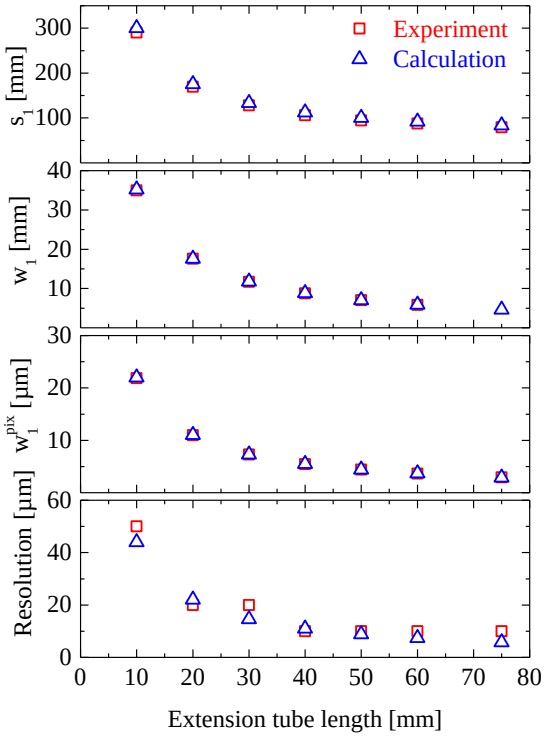

Figure 2: Measured (red squares) and calculated (blue triangles) performance data versus extension tube length of the telemicroscope: working distance s1, total horizontal field of view w1, horizontal field of view per pixel w1pix, and lateral resolution. The focusing length is f = 50 mm.

Camera, extension tube and lens are commercially devices. However, some vacuum-sensitive electronic parts had to be replaced. The resolution of the CCD camera is 1600 pixel x 1200 pixel. The overall dimension (including housing) is 60 x 70 x 210 mm^3. A sapphire window is used to protect the optics from direct particle impingement.

The performance of the telemicroscope was investigated using two test structures: a graticule structure for determining the field of view (see Reference [6]) and a special line structure for verifying the achievable lateral resolution. Both test structures are shown in Figure 3. The line structure consists of several pairs of lines. Each pair has five lines with equal width and spacing ranging from 10 µm up to 100 µm. As can be seen in Figure 3, all pairs of lines down to 10 µm can be resolved. Hence the lateral resolution of the telemicroscope is better than 10 µm.

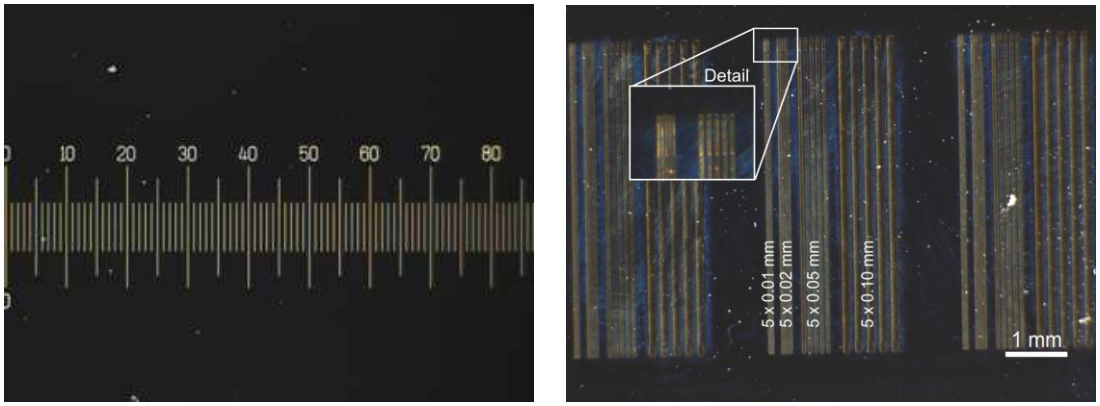

Figure 3: Telemicroscope image of test structures: graticule structure (left) and laser-scribed line structure (right).

In summary, performance evaluation revealed the following parameters: image size (field of view) is 8.75 x 6.56 mm^2 at a working distance of 112.5 mm, lateral (radial) accuracy is better than 0.01 mm, and depth of field (axial resolution) is better than 0.5 mm.

B. Triangular laser head

The triangular laser head measures the distance to an object upon exploitation of the triangulation effect (see Figure 4), i.e. a laser is directed onto the test object and the detector collects a fraction of the backscattered light. The detection angle is correlated with the distance. When scanning across an object of interest, the surface profile can be measured. This gives access to axial (and lateral) erosion.

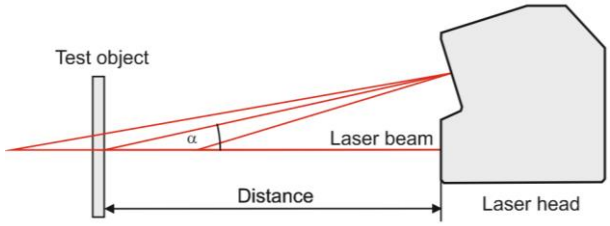

Figure 4: Sketch of the measurement principle of the triangular laser head (triangulation effect).

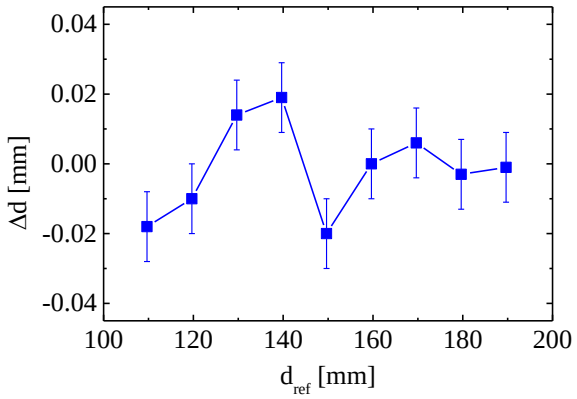

Figure 5: Difference between set distance and distance measured with the triangular laser head.

Similar to the telemicroscope, the triangular laser head was also placed inside a vacuum-sealed housing in the old setup. The housing contained not only the triangular laser head but also the pyrometer. The diameter and length of the housing was about 200 mm and 300 mm. The new design is shown in Figure 1. The triangular laser head is

now operated inside vacuum with a metal cover and sapphire windows. Thus, the dimension of the new setup is considerably smaller.

The triangular laser head is a commercial device. Again, vacuum-sensitive electronic parts had to be replaced. The distance measurement range covers 110 mm - 190 mm with a specified repeatability of better than 0.001 mm and distance resolution of better than 0.01 mm. The spot size is about 0.2 mm at a distance of 150 mm. The overall dimension of the setup (including housing) is 95 x 47 x 127 mm^3.

We performed principal tests of the triangular laser head using a high-precision linear table. The table was moved to certain positions. Then the measured distance is compared to the relative position change of the linear table. The results are plotted in Figure 5. The data show that the precision of the distance measurement is about 0.02 mm.

C. Pyrometer

The pyrometer is used to perform temperature spot measurements or line scans. The measurement principle is based on Planck's law, i.e. the intensity of the emitted infrared radiation depends on the object temperature, the emissivity of the object material, and the wavelength of radiation.

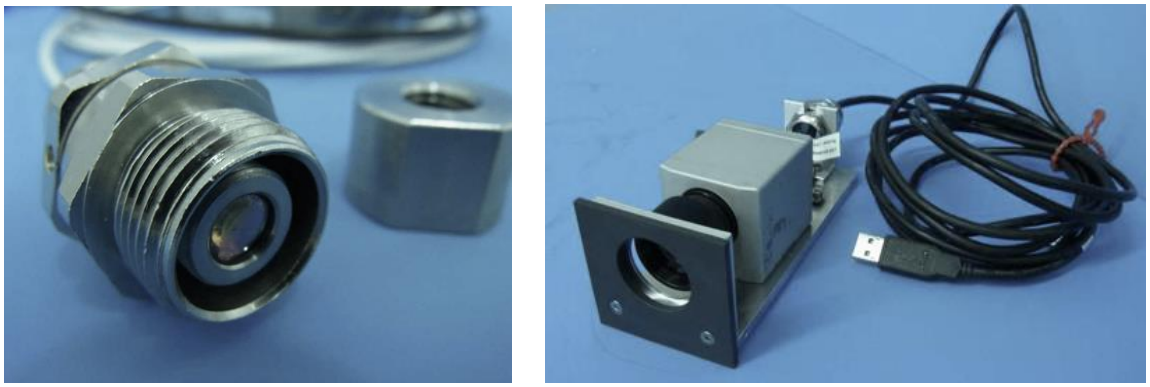

Figure 6: Pyrometer sensor head (left) and thermocamera (right) with housing.

The old setup used a device with a large vacuum sealed housing. Now, an alternative, much smaller device is used. The pyrometer sensor head including its housing is shown in Figure 6. The new pyrometer is operated inside vacuum. Due to the in-vacuum operation, vacuum-sensitive electronic parts had to be replaced or removed. A sapphire window is used in order to protect the pyrometer lens from direct impingement of energetic ions. Sapphire has not only a very good mechanical hardness but also a high transmission at the operation wavelength of the pyrometer ($t \sim 0.85$ at $\lambda = 2.3$ µm). The size of the measurement spot is 1.5 mm at the focal distance of 110 mm. Temperature range and resolution are 150°C – 1000°C and 0.1°C, respectively. The system accuracy and repeatability are given to be 0.3 % of reading + 2°C and 0.1 % of reading + 1°C, respectively. The overall dimension (including housing) is 25 x 30 x 47 mm^3.

D. Thermocamera

The thermocamera takes temperature images of objects of interest. As for the pyrometer, its measurement principle is based on Planck's law. The thermocamera uses a focal plane array as detector, which allows taking images. Typically, thermocameras are placed outside of the vacuum chamber. Due to the size of the chambers, the working distance is large and the achievable lateral resolution is limited. Here, the thermocamera is operated inside the vacuum chamber, which reduces the working distance and, thus, improves the lateral resolution.

The thermocamera is a commercial device and was chosen because of its small size. Again, some vacuum-sensitive electronic parts had to be replaced for in-vacuum operation. The thermocamera is protected by a metal cover and a ZnS window. The transmission of ZnS is $t = 0.75$ at $\lambda = 10$ µm.

The thermocamera operates in the spectral range from 7.5 µm to 13 µm. The image size is about 50 x 70 mm^2 at a working distance of 500 mm. The resolution of the camera is 160 pixels x 120 pixels. The lateral resolution is 1.5 mm. Temperature range and resolution is specified to be 0°C – 900°C and 0.1°C, respectively. The system accuracy is given to be 2 % of reading or 2°C. The overall dimension of the thermocamera (including housing) is 56 x 60 x 143 mm^3.

E. Retarding potential analyzer

The retarding potential analyzer is used to measure the energy distribution of charged particles. It is based on measuring the ion current I in dependence on the repelling voltage U (electrostatic energy analyzer). The (normalized) energy distribution is obtained by calculating the derivative of I(U).

The retarding potential analyzer (Figure 7) was developed in-house with the goal to make it as small as possible while keeping the performance (signal-to-noise ratio) sufficiently high. Therefore, a grid design with 149 holes has been chosen. The device consists of two grids and an ion collector. The first grid is used for focusing the ion trajectories, the second grid for repelling secondary electrons. The ion collector is used for measuring the ion current and for repelling the ions by applying a repelling voltage V.

The ion collector has cup-shaped cavities, one for each of the 149 ion channels. The repelling voltage can be varied between 0 V and 3000 V with accuracy better than 0.05 %. The collected ion current is transformed by a high-precision resistor into a voltage drop, which is measured by a 14-bit AD converter. The accuracy is better than 5 eV. The overall dimension of the device is 40 x 47 x 84 mm^3.

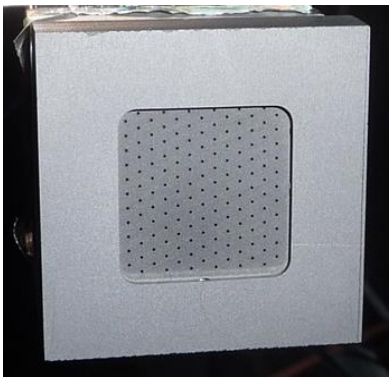

Figure 7: Front view of the retarding potential analyser.

F. Thruster

Test measurements were performed with a gridded ion thruster RIT-µX [9], which belongs to the class of radio-frequency ion thrusters (RITs). The thruster was operated with the standard propellant xenon at two operation points (see Table 1).

Table 1: Summary of operation parameters of the RIT-µX at two operation points (OPs).

Parameter	OP1	OP2
Beam Voltage	1050 V	1700 V
Beam Current	4 mA	8 mA
Nominal thrust	210 µN	540 µN

G. Test chamber

The tests were performed in the Jumbo test facility at Gießen University [10]. The tank is of cylindrical shape with a diameter of 2.6 m, a length of 6 m and a volume of 30 m^3. It is equipped with turbo and cryogenic pumps with a total pumping speed 65.000 l/s for xenon. The base pressure is about 1 x 10^{-7} mbar.

III. Results and Discussion

Because none of the manufactures of telemicroscope, triangular laser head, pyrometer or thermocamera have specified in-vacuum operation, we first performed principal in-vacuum tests. All devices were operated inside vacuum for at least 48 h. The tests were successful, i.e. all devices operated properly and stably. After that, the devices were tested with firing thrusters. In the following, selected test results with the RIT-µX thruster are presented.

H. Telemicroscope

Figure 8 shows a section of the grid at the beginning and at the end of the test campaign (total duration about 100 h). The grid holes can be clearly resolved and grid hole diameter and, hence, the grid hole erosion are accessible. The diameter of the center hole in Figure 8 is (1.27 ± 0.02) mm for both images. The two images demonstrate the repeatability and, reliability of the measurements.

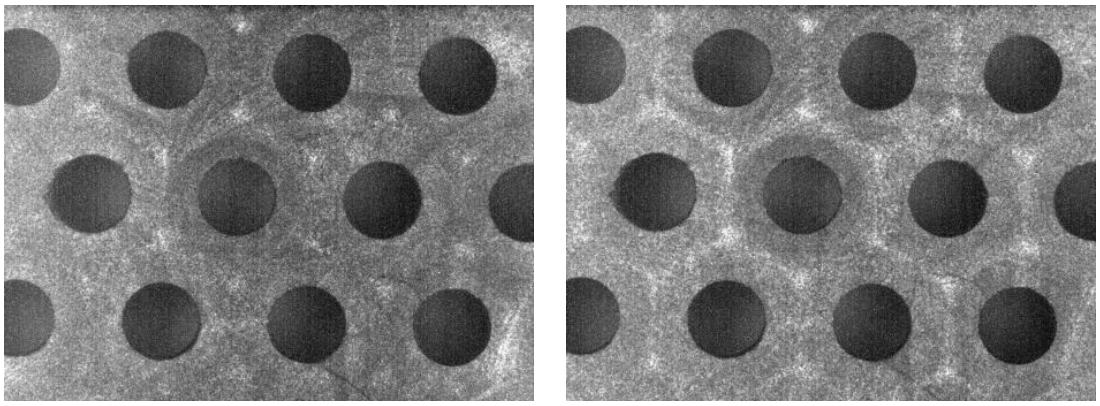

Figure 8: Telemicroscope images of grid holes of the RIT-µX before (left) and after the test campaign (right).

I. Triangular laser head

Figure 9 shows selected surface profile scans of the RIT-µX measured at different days. A very good repeatability can be seen. The extraction grid hole area can be identified clearly and the number of holes can be seen. Doing so, the principal shape of the grid including its radius of curvature could be measured, as demonstrated recently for a gridded ion thruster RIT-22 [2,3]. The grids of the RIT-µX are flat.

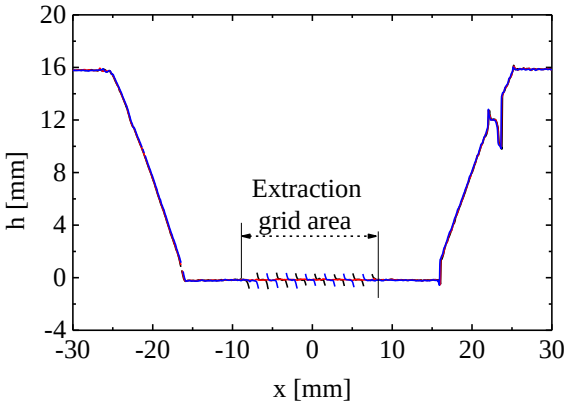

Figure 9: Surface profile scans across the center of the RIT-µX measured with the triangular laser head. There are three lines representing measurements from three different days.

However, there are experimental limitations due to the measurement principle (triangulation effect), i.e. the triangular laser head might fail in measuring steep or abrupt edges (see the sharp structures in the extraction grid area in Figure 9).

J. Thermocamera

Figure 10 shows thermocamera images of the RIT-µX. The surface temperature of almost the whole thruster is imaged. The surface temperature distribution of the grid is nearly homogeneous, apart from the holes, which is caused by the fact that the temperature of the plasma chamber, which is imaged through the holes, is considerably higher than the grid surface temperature [2,3]. In Figure 11 temperature line scans across the center of the thruster are plotted. The grid temperature was found to be $(62° \pm 2)°C$ at operation point 1 and $(68° \pm 2)°C$ at operation point 2.

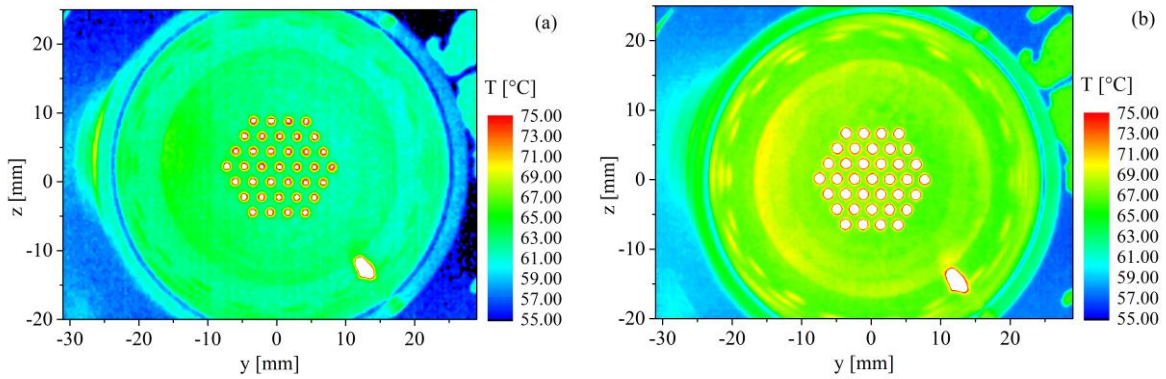

Figure 10: Thermocamera images of the RIT-µX at OP1 (a) and OP2 (b).

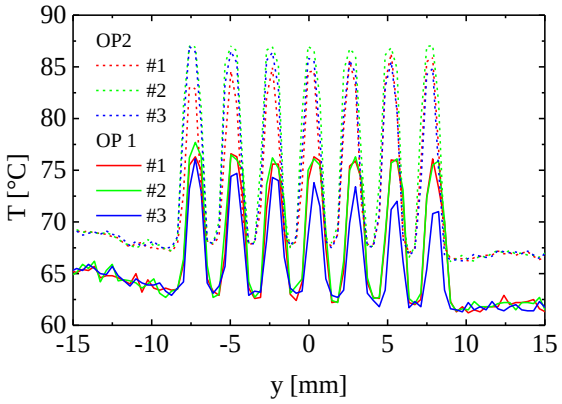

Figure 11: Horizontal temperature scans across the center of the RIT-µX at OP1 (solid lines) and OP2 (dashed lines) extracted from thermocamera images. Different lines represent different z-positions.

K. Retarding potential analyzer

Figure 12 shows selected energy distributions measured with the retarding potential analyzer at certain time steps at different days.

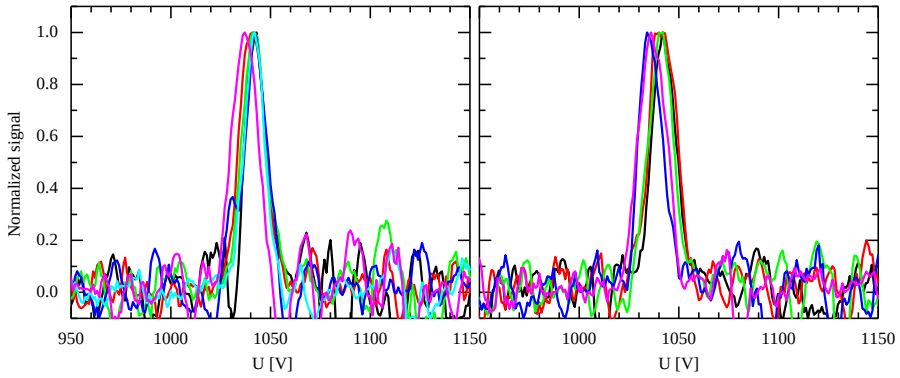

Figure 12: Energy distributions of the RIT-µX at OP1 measured with the retarding potential analyser at two different days (day 1: left; day 2: right).

All curves reveal a single peak, which is typical for gridded ion thrusters. The shape of the peaks is Gaussian like and very similar for all measurements. However, the peak position scatters between 1038 eV and 1046 eV. This is

tentatively assigned to the fact that the peak position is mainly determined by the beam voltage but also by the plasma potential and the secondary star ground. Still, the scattering is less than 1 % of the ion energy. The width at half maximum of the peak is smaller than 20 V, which corresponds to less than 2 % of the ion energy. Ions with other energies, e.g. generated by charge exchange processes, were not detected. The data show a good repeatability and reliability. However, the curves in Figure 12 are very noisy. Therefore, the electronics needs some further improvements with regard to signal-to-noise ratio.

IV. Summary and Outlook

We have reported about the new design of our diagnostic tools for in-situ EP thruster characterization, including probes for beam characterization (retarding potential analyzer), thermal characterization (pyrometer, thermocamera) and optical inspection (telemicroscope, triangular laser head).

The designs have been improved with respect to certain problems, which we noticed with the AEPD1 platform. We are now operating all diagnostic tools, for the very first time, inside vacuum. Because of that, the size of the diagnostic tool setups could be reduced considerably, which reduces the interaction with the energetic particle beam of the thruster. Moreover, the risk of a vacuum breakdown is eliminated completely. We demonstrated that the tools operate well in the vacuum environment with a firing thruster, even though they are mostly not specified for in-vacuum operation, and provide reliable and reproducible results.

Acknowledgments

The work was performed with financial support provided by ESA/ESTEC (contract No. 4000107451/12/NL/RA; ”Qualification of the AEPD System as a Standard On-Ground Tool for Electric Propulsion Thrusters”). The authors thank R. Woyciechowski, M. Müller, S. Daum (all Leibniz-Institute of Surface Modification), R. Kukies (Airbus Defence & Space), W. Gärtner, U. Bachmann (all Justus-Liebig-Universität Gießen) for technical support. We are greatly indebted to our project coordinators at ESA/ESTEC, A. Bulit, K. Dannenmayer, D. Feili and J. Gonzalez del Amo.

References

[1] C. Bundesmann, M. Tartz, F. Scholze, H.J. Leiter, F. Scortecci, R.Y. Gnizdor, H. Neumann, Rev. Sci. Instrum., Vol. 81, 23 April 2010, 046106, pp. .

[2] C. Bundesmann, M. Tartz, F. Scholze, H. Neumann, H.J. Leiter, F. Scortecci, D. Feili, P.E. Frigot, J. Gonzalez del Amo, *Proceedings of the 31st International Electric Propulsion Conference*, Ann Arbor, 2009, Paper IEPC-2009-160.

[3] C. Bundesmann, M. Tartz, F. Scholze, H. Neumann, H.J. Leiter, F. Scortecci, J. Propul. Power, Vol. 27, Nr. 3, May-June 2011, pp. 532-537.

[4] C. Bundesmann, M. Tartz, F. Scholze, H. Neumann, F. Scortecci, S. Scaranzin, P.E. Frigot, J. Gonzalez del Amo, R.Y. Gnizdor, *Proceedings of the 31st International Electric Propulsion Conference*, Ann Arbor, 2009, Paper IEPC-2009-141.

[5] D. Pagano, F. Scortecci, C. Bundesmann, C. Eichhorn, F. Scholze, H. Neumann, H. Leiter, H. Kersten, S. Gauter, R. Wiese, R. Blott, P.J. Klar, K. Holste, B. Meyer, S. Mazouffre, A. Bulit, J. Gonzales del Amo, *Proceedings of the 34th International Electric Propulsion Conference*, Hyogo-Kobe, 2015, Paper IEPC-2015-363.

[6] C. Bundesmann, C. Eichhorn, F. Scholze, D. Spemann, H. Neumann, D. Pagano, S. Scaranzin, F. Scortecci, H.J. Leiter, S. Gauter, R. Wiese, H. Kersten, K. Holste, P. Köhler, P.J. Klar, S. Mazouffre, R. Blott, A. Bulit, K. Dannenmayer, J. Gonzales del Amo, *Proceedings of 5th Space Propulsion Conference*, Roma, 2016, Paper SP2016_3124997.

[7] C. Bundesmann, C. Eichhorn, F. Scholze, H. Neumann, H.J. Leiter, F. Scortecci, *Proceedings of the 34th International Electric Propulsion Conference*, Hyogo-Kobe, 2015, Paper IEPC-2015-392

[8] C. Bundesmann, C. Eichhorn, F. Scholze, D. Spemann, H. Neumann, D. Pagano, S. Scaranzin, F. Scortecci, H.J. Leiter, S. Gauter, R. Wiese, H. Kersten, K. Holste, P. Köhler, P.J. Klar, S. Mazouffre, R. Blott, A. Bulit, K. Dannenmayer, *Eur. Phys. J. D*, Vol. 70, No. 217, 18 October 2016, pp. 1-11.

[9] C. Altmann, H. Leiter, R. Kukies, *Proceedings of the 34th International Electric Propulsion Conference*, Hyogo-Kobe, 2015, Paper IEPC-2015-274.

[10] P.J. Klar, K. Hannemann, U. Ricklefs, H. Leiter, *Proceedings of the 34th International Electric Propulsion Conference*, Hyogo-Kobe, 2015, Paper IEPC-2015-89.